Urban Aerosol Characteristics during the World Expo 2010 in Shanghai

Min Zhang, Jianmin Chen, Xianyao Chen, Tiantao Cheng, Yuanling Zhang, Hefeng Zhang, Aijun Ding, Meng Wang, Abdelwahid S Mellouki

Aerosol and Air Quality Research, 13: 36–48, 2013

ISSN: 1680-8584 print / 2071-1409 online
doi: 10.4209/aaqr.2012.02.0024

Urban Aerosol Characteristics during the World Expo 2010 in Shanghai

Min Zhang[1,2], Jianmin Chen[1*], Xianyao Chen[2†], Tiantao Cheng[1], Yuanling Zhang[2], Hefeng Zhang[3], Aijun Ding[4], Meng Wang[2], Abdelwahid Mellouki[3]

[1] *Department of Environmental Science and Engineering, Fudan University, Shanghai 200433, China*
[2] *Key Laboratory of Data Analysis and Application, The First Institute of Oceanography, State Oceanic Administration, Qingdao 266061, China*
[3] *ICARE-CNRS/OSUC, 1C Avenue de la Recherche scientifique, 45071 Orleans cedex 02, France*
[4] *School of Atmospheric Sciences, Nanjing University, Nanjing 210093, China*

ABSTRACT

During the World Exposition 2010, which ran from May to October, emission control measures were implemented in Shanghai and surrounding areas to improve the air quality. This study evaluated the effects of regional transport on aerosol characteristics under these controlled local emission conditions using a month's worth of observations of the aerosol number size distributions (10 nm–10 μm) and the chemical compositions of the aerosols. Back-trajectories and a Lagrangian dispersion model were combined to analyze the transport characteristics of regional and local air pollution and the related mechanisms. Two classes of aerosols were identified and compared. Class I was a clear air condition with ocean-oriented air masses. Particle counts in this class were dominated by particles in the size range 20–40 nm, and NH_4^+ was mainly present in the form of $(NH_4)_2SO_4$. A strong peak at noontime indicated that the particle formation or growth process was promoted by the photochemical process. Class II was characterized as a regional transport pollution condition with air masses originating in the surrounding areas. The analysis showed increases in particle number concentrations and total water soluble ions of about 17% and 350%, respectively, compared with Class I episodes. The fraction of particles in the size range 50–200 nm increased sharply to almost 50% of the total particle counts. An examination of the diurnal pattern and major water soluble ions suggested that the increase in size mode (50–200 nm) particles was mainly due to the particle growth process and the presence of enough precursor gases. NH_4^+ was present in the form of $(NH_4)_2SO_4$ and NH_4NO_3. Although air control measures during the World Expo significantly limited local emissions, our results indicate that the regional transport from surrounding cities was responsible for the higher trace gases and particle volume concentrations, along with the large number of Aitken mode particles.

Keywords: Shanghai World Expo; $PM_{2.5}$; Particle number size distribution; Chemical composition; Lagrangian model.

INTRODUCTION

Shanghai, with a population of over 20 million, is one of the largest cities in China. During the past several decades, rapid increasing industrial and metropolitan emissions have caused a deterioration in Shanghai's air quality. Recent satellite measurements (GOME and SCIAMACHY) have shown that in the 1996–2005 period, there was a yearly increase of 20% ± 6% in the tropospheric NO_2 columns over Shanghai (Van der *et al.*, 2006). The annual average $PM_{2.5}$ concentrations increased from about 60 μg/m^3 in1999–2000 to about 90 μg/m^3 in 2005–2006 (Ye *et al.*, 2003; Feng *et al.*, 2009). As the adverse health effects of fine particles increase rapidly with expanding population size (Kan *et al.*, 2007) and the air pollution output from mega-cities in China is now considered to be a global concern (Chan and Yao, 2008), air pollution, especially the fine particle characterization in the Shanghai metropolitan area, has become a hot research topic.

The World Expo 2010 was hosted in Shanghai from May 1 to October 31, 2010. It was the other most important international event in China, after the 2008 Olympic Games in Beijing. Of special concern was the air quality in six month during the World Expo that the visitors from all over the world would face to. To improve the city's air quality during the World Expo, the Shanghai government took drastic action to reduce air pollutant emissions from energy, industry, transport and construction sources in Shanghai and the surrounding cities (UNEP, 2010). In particular, open

* Corresponding author. Tel.: +86 21 6564 2298
E-mail address: jmchen@fudan.edu.cn
† Corresponding author. Tel.: +86 532 8896 7691
E-mail address: chenxy@fio.org.cn

biomass burning was strictly forbidden during the World Expo (Zhang *et al.*, 2008; Li *et al.*, 2010; Du *et al.*, 2011; Zhang *et al.*, 2011). Satellite measurements (GOME, MODIS and MOPITT) have verified that these air quality control measures were effective (Hao *et al.*, 2011; Jia *et al.*, 2012). These circumstances make Shanghai during the World Expo a good case study for the physical and chemical characterizations of aerosol particles under controlled local emission conditions.

Since ultra-fine and fine particles play a key role in air pollution in Shanghai (Mönkkönen *et al.*, 2005; Tie *et al.*, 2006; Streets *et al.*, 2008; Yang *et al.*, 2009; Wang *et al.*, 2010; Li *et al.*, 2011; Ye *et al.*, 2011; Fu *et al.*, 2012), the in-situ characterization of the chemical and physical properties of atmospheric fine particles is essential to the evaluation of the air pollution level under controlled local emission conditions. Aerosol size and size distribution are important aspects of aerosol physical properties, and the particle number concentration of fine particles should get more attention than the mass concentration (Tsai *et al.*, 2011; Gómez-Moreno, 2011; Ny and Lee, 2011; Du *et al.*, 2012). Previous studies of particle size distribution in Shanghai have shown that the average particle number concentrations (10–100 nm) are 2–3 times higher than those reported in the urban areas of North America and Europe (Kulmala *et al.*, 2004; Gao *et al.*, 2009). The diurnal pattern is strongly influenced by local sources such as traffic density and nucleation (Du *et al.*, 2012). A number of papers have been published on the air quality changes during the Olympic Games in Beijing. The pollution control measures during the Olympic Games lead to decreases in water-soluble ions, black carbon and trace gases (Wang *et al.*, 2009a; Wang *et al.*, 2009b; Zhou *et al.*, 2010; Okuda *et al.*, 2011; Li *et al.*, 2012), but fine particles ($PM_{2.5}$) were not effectively reduced (Wang *et al.*, 2009b; Okuda *et al.*, 2011).

The objective of this study was to obtain an in-situ characterization of the chemical and physical properties of atmospheric fine particles during one month of the World Expo, under controlled local emission conditions. We deployed an online analyzer to monitor water-soluble ions and trace gases and a wide-range particle spectrometer to measure the particle number size distributions of ambient submicron particles with high time resolution. Back-trajectories and Lagrangian model analyses were combined to differentiate and compare the regional transport and local contributions. The World Expo provided an unique opportunity to examine the fine particle pollution in Shanghai under controlled local emission conditions. The results of this study will help researchers and policy-makers to determine the effectiveness of local environmental control measures on atmospheric fine particle pollution.

EXPERIMENTAL

Sampling Site

In-situ measurements were performed continuously on the rooftop of a six-story building (about 20 m above the ground) within the Handan campus of Fudan University in Shanghai (31°18'N, 121°29'E). The sampling site, roughly 20 km northeast of the city center, was chosen as a representative urban district due to the mixed influence of residential, construction and traffic emissions. Surrounding Shanghai are three provinces-Jiangsu, Anhui, and Zhejiang (Fig. 1). All dates and times were reported in the local time (LT), which is 8 h ahead of UTC.

Instrumentation and Measurements

Particle number size distribution was measured online by a Wide-range Particle Spectrometer (WPS^{TM}-model 1000 XP, MSP Corporation, USA), with a wide size range from 10 nm to 10 μm. The instrument consists of a high-resolution Differential Mobility Analyzer (DMA), a Condensation Particle Counter (CPC) and a wide-angle Laser Particle Spectrometer (LPS). The DMA and CPC can measure the aerosol size distribution in the 10–500 nm range up to 96 channels. The LPS covers the 350–10,000 nm range in 24 additional channels.

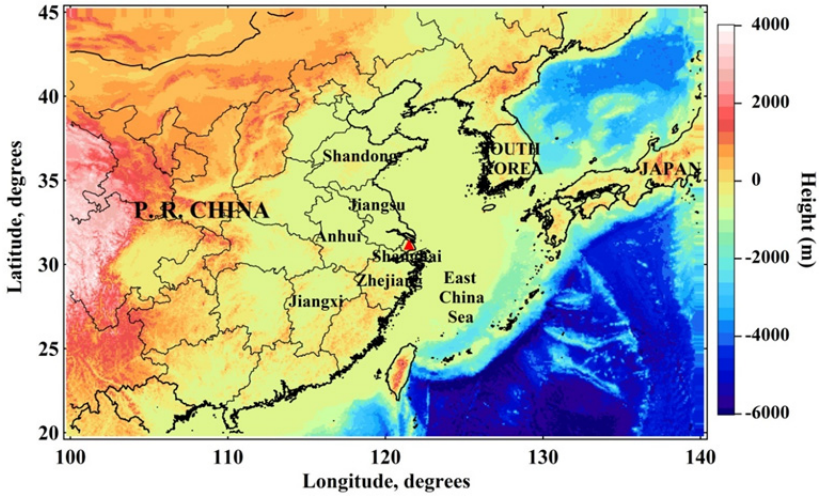

Fig. 1. Location of the sampling site in Shanghai (red triangle) and the surrounding cities with the topography (shown by color shading) displayed in the figure for reference.

In this study, we chose the sample mode with 60 channels in DMA and 24 channels in LPS. One complete scan of the entire size range, with a 2 s scanning period for each channel, took approximately 3 min. Volume size distributions were calculated from number size distributions by assuming spherical particles. The daily arithmetic mean particle density was generally between 1.5 and 2.0 g/cm^3 in Shanghai (Zhang *et al.*, 2010), here we chose 1.7 g/cm^3 as the average particle density for the calculation from volume size distribution to $PM_{2.5}$ mass concentrations. Detailed information can be found in Liu *et al.* (2010) and Zhang *et al.* (2010).

A model ADI 2080 online analyzer for the Monitoring of AeRosols and GAses (MARGA, Applikon Analytical B.V. Corp., the Netherlands) with a $PM_{2.5}$ sampling inlet was used to conduct intensive measurements of particulate water-soluble ions. The MARGA instrument, developed and verified by an energy research center in the Netherlands, consists of sampling and analytical boxes (Jongejan *et al.*, 1997). The sample box is comprised of a Wet Rotating Denuder (WRD) and a Steam Jet Aerosol Collector (SJAC). Compared with traditional sampling methods, such as filter-pack sampling (Khlystov *et al.*, 1995; Chow *et al.*, 1998), the MARGA is an effective and sound tool for absorbing gas and collecting aerosols (sampling efficiency of 99%). The MARGA system has the capability of measuring mass concentrations of major water-soluble inorganic ions (NH_4^+, Na^+, K^+, Ca^{2+}, Mg^{2+}, SO_4^{2-}, NO_3^-, Cl^-) and trace gases (HCl, HONO, SO_2, HNO_3, NH_3) at a 1-h time resolution. To track changes in retention time and detector response for each sampling, the MARGA was continuously controlled by an internal calibration method using bromide for the anion chromatograph and lithium for the cation chromatograph over the entire observation period (Detailed description of this process can be found in Du *et al.* 2010 and Du *et al.*, 2011).

O_3 and NO-NO_2-NO_x were measured with a model 49i ozone analyzer and a model 42i NO-NO_2-NO_x analyzer (Thermo Fisher Scientific, Co., Ltd.), respectively. These instruments were automatically set to zero and have external calibration sources that meet the technical specifications for the US Environmental Protection Agency (EPA) (http://www.epa.gov/ttn/amtic/criteria.html).

Meteorological parameters such as wind speed/direction, relative humidity, ambient temperature and pressure were automatically recorded by a Kestrel 4000 pocket weather tracker (Nielsen-Kellermann Inc., USA).

Daily values for the Air Pollution Index (API) were acquired from the Shanghai Environmental Monitoring Center (http://www.semc.gov.cn/). The API is a semi-quantitative measure for uniformly reporting air quality in China, and it is based on a set of atmospheric constituents that have implications for human health. Detailed information can be found in Qu *et al.* (2010).

FLEXPART and HYSPLIT Models

To simulate and diagnose the air mass origins and transport/dispersion processes for different air quality episodes, we employed a Lagrangian particle dispersion model, FLEXPART (Stohl *et al.*, 1998; Stohl *et al.*, 2005) (see http://zardoz.nilu.no/_andreas/flextra+flexpart.html). FLEXPART releases so-called tracer particles at emission sources or receptors and calculates their trajectories using the mean winds interpolated from the meteorological input fields, plus random motions representing turbulence. This model has been widely used in the analysis of data for atmospheric chemistry experiments to investigate the influence of various meteorological processes on pollution transport, such as tracing the long-range transport of biomass burning emissions (Fiebig *et al.*, 2009), sources attribution (local or regional) (Quinn *et al.*, 2006) and dispersion over complex terrains (De Foy *et al.*, 2006; Palau *et al.*, 2006). A special feature of FLEXPART is the possibility of running it backward in time to produce information on the spatial distribution of sources contributing to a particular measurement (Stohl *et al.*, 2003; Seibert *et al.*, 2004).

For this study, backward air mass trajectories were produced using the Hybrid Single-Particles Lagrangian Integrated Trajectory (HYSPLIT4) model available at the NOAA/ARL's (US National Oceanic and Air Administration/Air Resources Laboratory) web server (Draxler and Hess, 1998). The Global Data Assimilation System (GDAS) was used for the trajectory calculation (http://www.arl.noaa.gov/ready/hysplit4.html).

RESULTS AND DISCUSSION

Overview

This analysis of aerosol characteristics under controlled local emission conditions in Shanghai used measurements of atmospheric particle number size distributions and $PM_{2.5}$ chemical compositions collected in August 2010 during the World Expo. The variations in API values, $PM_{2.5}$ mass concentrations and total particle number concentrations are presented in Fig. 2. An interesting alternation with a 5–7 day cycle between air quality Class I (API $\leq$ 50) and Class II (API = 51–100) was observed. Class II episodes were characterized by elevated $PM_{2.5}$ levels, which were 2–3 times higher than during the Class I episodes. While the peak particle counts in both Classes were above 2×10^4 cm^{-3}.

A detailed examination of the aerosol number size distributions and concentrations of total water-soluble ions during the entire month are shown in Fig. 3. Two typical shapes were found, each with a 5–7 day cycle, which was consistent with the variations in API and $PM_{2.5}$. The particle number size distributions were dominated by particles in the size ranges of 20–40 nm and 50–200 nm during the Class I episodes (6–9 August and 19–26 August) and Class II episodes (1–4 August, 12–16 August and 27–31 August), respectively (Fig. 3(a)). Unlike the new particle formation process that has been reported in previous studies (Gao *et al.*, 2009; Gao *et al.*, 2011; Du *et al.*, 2012), few nucleation mode particles (10 nm) were observed, which was consistent with the observations made during the special pollution control period in Beijing (Gao *et al.*, 2012). The elevation of total water-soluble ions (mainly NO_3^-, SO_4^{2-} and NH_4^+) could have been responsible for the larger particle size range during the Class II episodes. The summary statistics of the ion species showed that the NO_3^-, SO_4^{2-} and NH_4^+

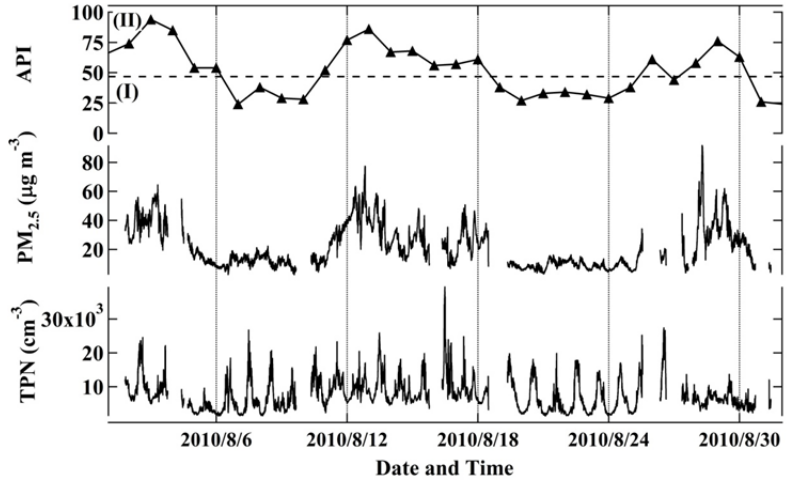

Fig. 2. Variations in API values, $PM_{2.5}$ and total particle number concentrations (TPN) in August 2010.

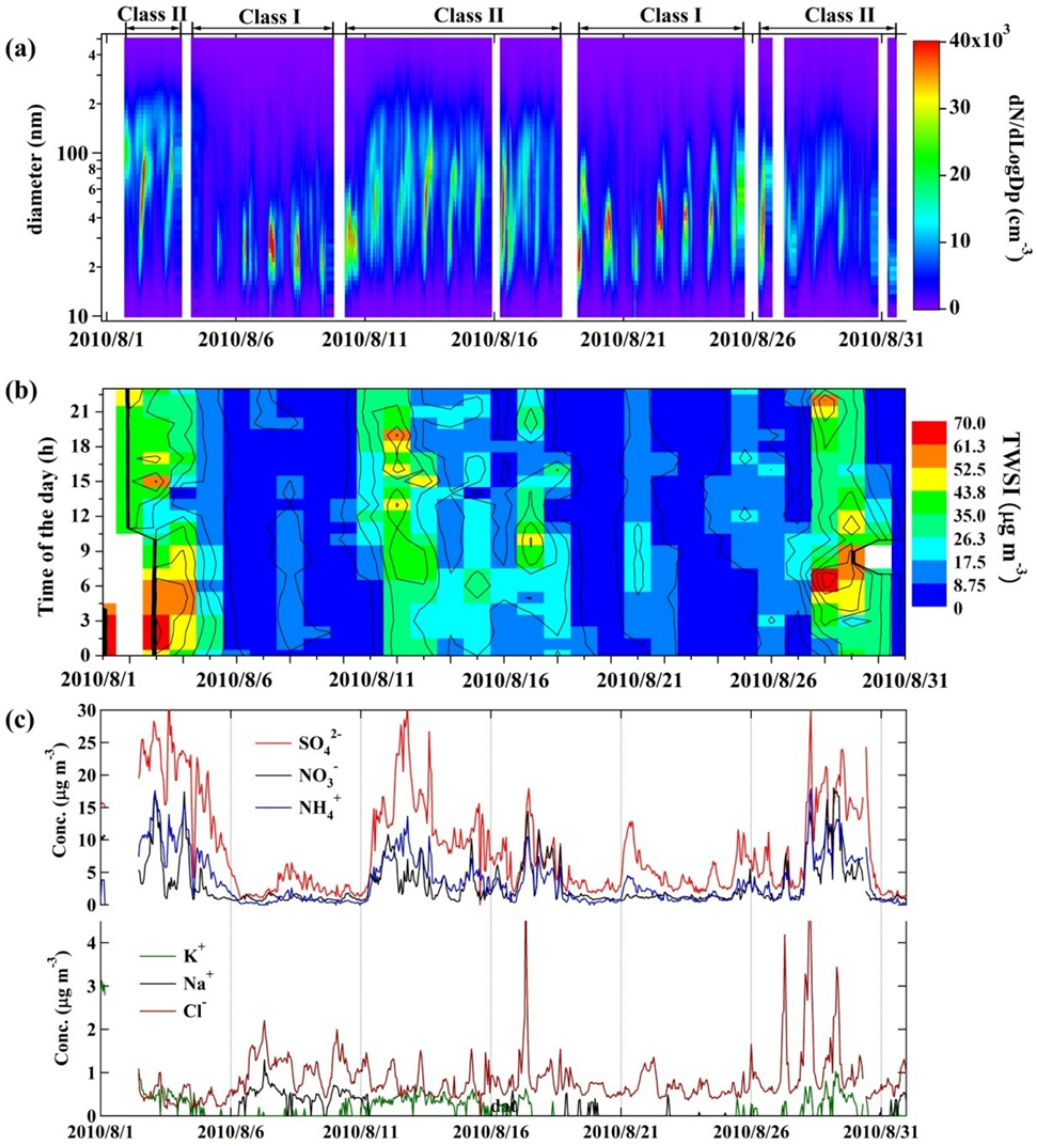

Fig. 3. Time series of (a) number size distributions, (b) total water-soluble ion concentrations and (c) major water-soluble ion concentrations in August 2010. Gaps in the data are the result of the non-availability of data in those periods due to adverse weather conditions or the cleaning of the instruments.

concentrations in the Class II episodes were close to 4–10 times higher than in the Class I episodes (Table 1).

Based on particle diameter, we classified particle size into the following modals: nucleation (10–20 nm), Aitken (20–100 nm), accumulation (100–1000 nm) and coarse (1–10 μm) modes. Table 2 summarizes the statistics of particle number concentrations in different size ranges for air quality Classes I and II. The average number concentrations of particles integrating for full sizes were much less than 1×10^4 cm^{-3} in both Classes I and II. These values were much lower than previous measurements at the same site (Du *et al.*, 2012). The particle counts within the 10–500 nm range were lower than those measured in rural areas of Pittsburgh and much lower than previously reported results from other urban and suburban areas (Gao *et al.*, 2009). In fact, the total number concentrations for Class II showed a higher variability, with a range of 1.4×10^3 cm^{-3} to 3.9×10^4 cm^{-3}, than the number concentrations in Class I. Particles of nucleation and Aitken modes were predominant in the entire size range for Class I with fractions of 13.5% and 73.7%, respectively, whereas Aitken and small accumulation (100–200 nm) modes for Class II had fractions of 65.3% and 21.5%, respectively.

Local/Regional Sources Attribution

The two size ranges and the different chemical compositions indicated different sources for the particles in the Class I and Class II episodes. To determine the effect of different source regions on aerosol size and chemical composition, five-day air mass back-trajectories were calculated using the HYSPLIT model at 200 m above the starting point (Fig. 4). Based on the transport pathways of air masses, two types of air masses were found, corresponding to air quality Classes I and II. The analysis showed that Class I air masses originated in the East China Sea and carried the clean air to the sampling site, whereas Class II air masses passed over highly polluted areas (such as Anhui, Jiangxi, Zhejiang, Shandong and Jiangsu) before arriving at the sampling site, where they may have influenced ground-level air quality. Thus, the most likely reason for the alternation between air quality Classes I and II was the circulation of these two air masses.

To compare and diagnose the possible source regions (local or regional) of the three Class II episodes (1–4 August, 12–16 August and 27–31 August), we applied the Lagrangian particle dispersion model (FLEXPART) in a backward mode (Fig. 5). The results showed that during the first two episodes (1–4 August and 12–16 August) most of the emissions were local, 80% and 71%, respectively. Volume concentrations from these two episodes were in the range of 10–45 $\mu m^3/cm^3$ and particle size bin 100–500 nm was the major contributor (around 60%). The total particle number concentrations for the 1–4 August and 12–16 August episodes were mostly in the range of $1–3 \times 10^4$ cm^{-3} and particle size bins 20–100 nm and 100–500 nm were the major contributors. For the last episode, (27–31 August), the transport pathway of the air masses was different than in the previous two periods, with only about 30% from local emissions. The air masses lingered over northern China, mainly passing over Shandong and Anhui provinces, which are often heavily polluted. The major difference in the composition of this air mass was the larger proportion of 500–1000 nm particles in the total volume concentration and the increased proportion of 20–100 nm to the total particle number concentrations. Compared with the 1–4 August and 12–16 August episodes, the 27–31 August episode was characterized by higher Cl^- and NO_3^- concentrations (Fig. 3(c)) and relatively higher SO_2 (data

Table 1. Mean concentrations ($\mu g/m^3$) of major aerosol water-soluble ions and total water-soluble ions during the Class I and Class II episodes.

Air Quality	Episodes	Cl^-	NO_3^-	SO_4^{2-}	Na^+	NH_4^+	K^+	Mg^{2+}	Ca^{2+}	TWSI
Class I	Aug. 6−9	1.07	1.00	2.87	0.43	0.73	0.01	0.25	0.89	7.25
Class I	Aug. 19−26	0.66	1.33	4.64	0.02	1.50	0.01	0.10	0.60	8.86
Class II	Aug. 1−4	0.45	6.31	21.61	0.00	10.31	0.41	0.21	1.09	40.39
Class II	Aug. 12−16	0.73	4.60	17.99	0.00	7.51	0.41	0.10	0.80	32.13
Class II	Aug. 27−31	1.43	8.04	16.66	0.00	8.75	0.36	0.07	0.65	34.75

Table 2. Descriptive statistics of the measured particle number concentrations (cm^{-3}) in different ranges for air quality Classes I and II.

Size bins	Mean		Percentage (%)		Max		Min		SD	
	I	II	I	II	I	II	I	II	I	II
10−20 nm	924	551	13.48	6.84	10,580	7280	93	48	956	526
20−50 nm	3608	2865	52.64	35.58	17,328	21,509	381	325	3303	2447
50−100 nm	1441	2394	21.02	29.73	10,843	16,566	287	340	1250	1830
100−200 nm	710	1733	10.36	21.52	5563	8600	139	180	620	1068
200−500 nm	164	474	2.39	5.89	881	1498	25	42	136	287
0.5−1 μm	6	36	0.09	0.45	37	191	1	1	6	29
1−10 μm	1	2	0.01	0.02	3	11	0	0	1	1
10−500 nm	6847	8016	99.90	99.54	26772	39473	1361	1370	4708	4550
Total	6854	8053	100	100	26,778	39,486	1364	1377	4708	4548

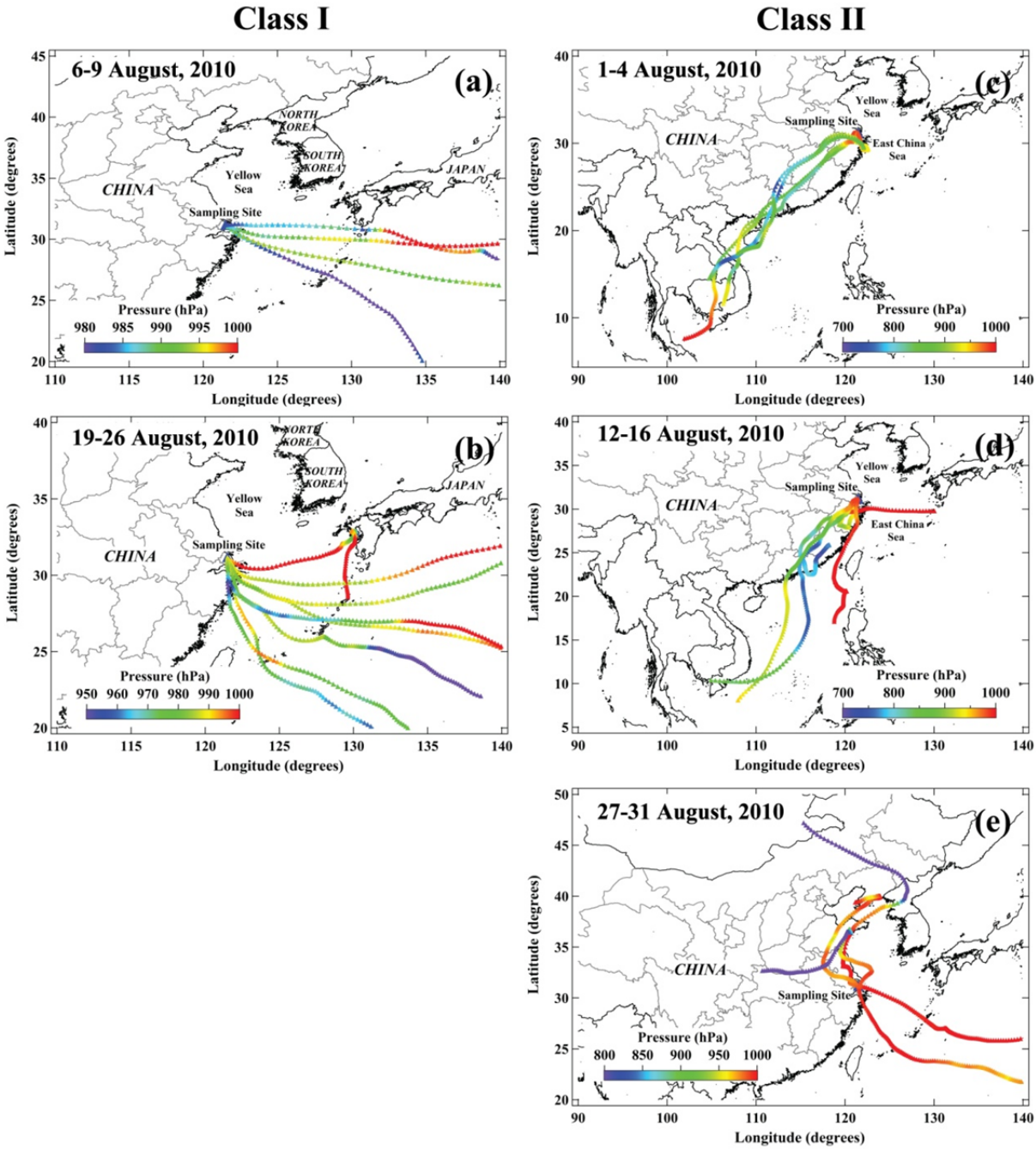

Fig. 4. The five-day back-trajectories of air masses arriving in Shanghai for Class I (a, b) and Class II (c, d, e) episodes.

not shown) and sulfur oxidation ratios (SOR, Fig. 7), which were probably beneficial to the particle growth process. Thus, it can be deduced that long-range transport from Anhui and Shandong provinces increased the number of Aitken-mode particles and brought more particles in the size range of 100–500 nm. Alternately, these particles could have been formed during the subsequent particle growth processes, which also contributed to larger volume concentrations.

Class I versus Class II

Based on the local/regional attribution analysis above, Class I episodes could be regarded as clear air conditions with ocean-oriented air masses, whereas Class II episodes were the result of pollution from regional transport and local sources mixed with air masses originating in surrounding cities. To better understand the characteristics of the aerosol number size distributions and the formation mechanisms for the two classes of air quality, Class I and Class II, under controlled local emission conditions, we compared two typical and consecutive cases (6–9 August and 12–16 August) for Class I and Class II, respectively. As the air mass back-trajectory for the 12–16 August episode was the most polluted air mass (Huang *et al.*, 2012), it was chosen for further comparison and discussion.

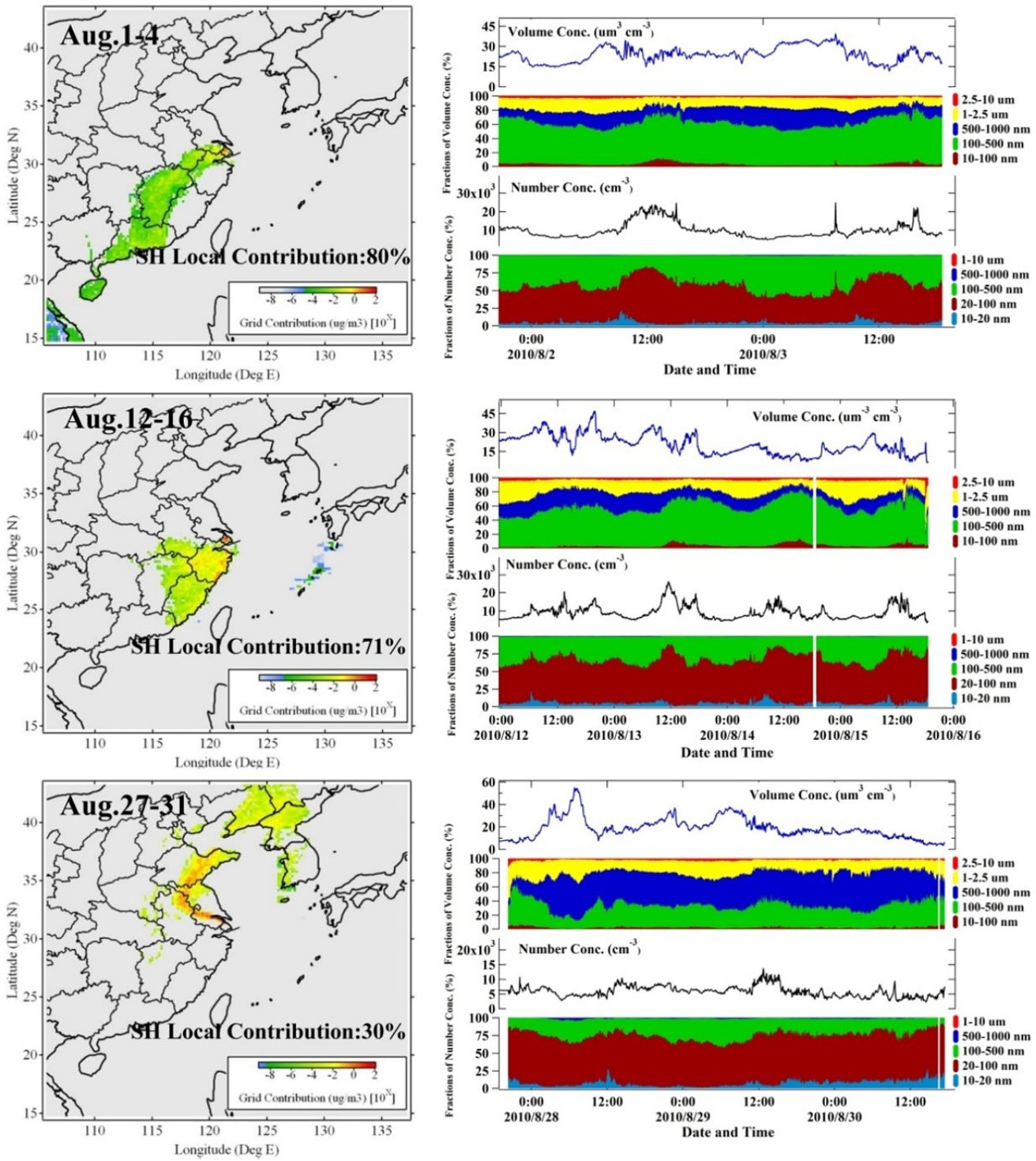

Fig. 5. (Left) sources attributions from the Langarian model analysis; (Right) total number concentrations, mass concentration and ratios of different particle size bins for Class II episodes in 1–4 August (top), 12–16 August (middle), 27–31 August (bottom).

The number size distributions, number and volume concentrations and the fractions of different particle size bins for these two episodes (6–9 August and 12–16 August) are shown in Fig. 6. The particle number size distribution was dominated by particles in the size range 20–40 nm for the 6–9 August episode (Class I) (Fig. 6(a)). Nucleation and Aitken mode particles were the main contributors to the total particle number concentration (Fig. 6(c)). A closer look at the diurnal variations in the average number concentrations of nucleation, Aitken and accumulation particles (Fig. 7) and nucleation and Aitken mode particles revealed a diurnal pattern similar to that of the total particle number concentrations, with peaks occurring midday (10:00–15:00). The sharp increase in particle number concentrations at

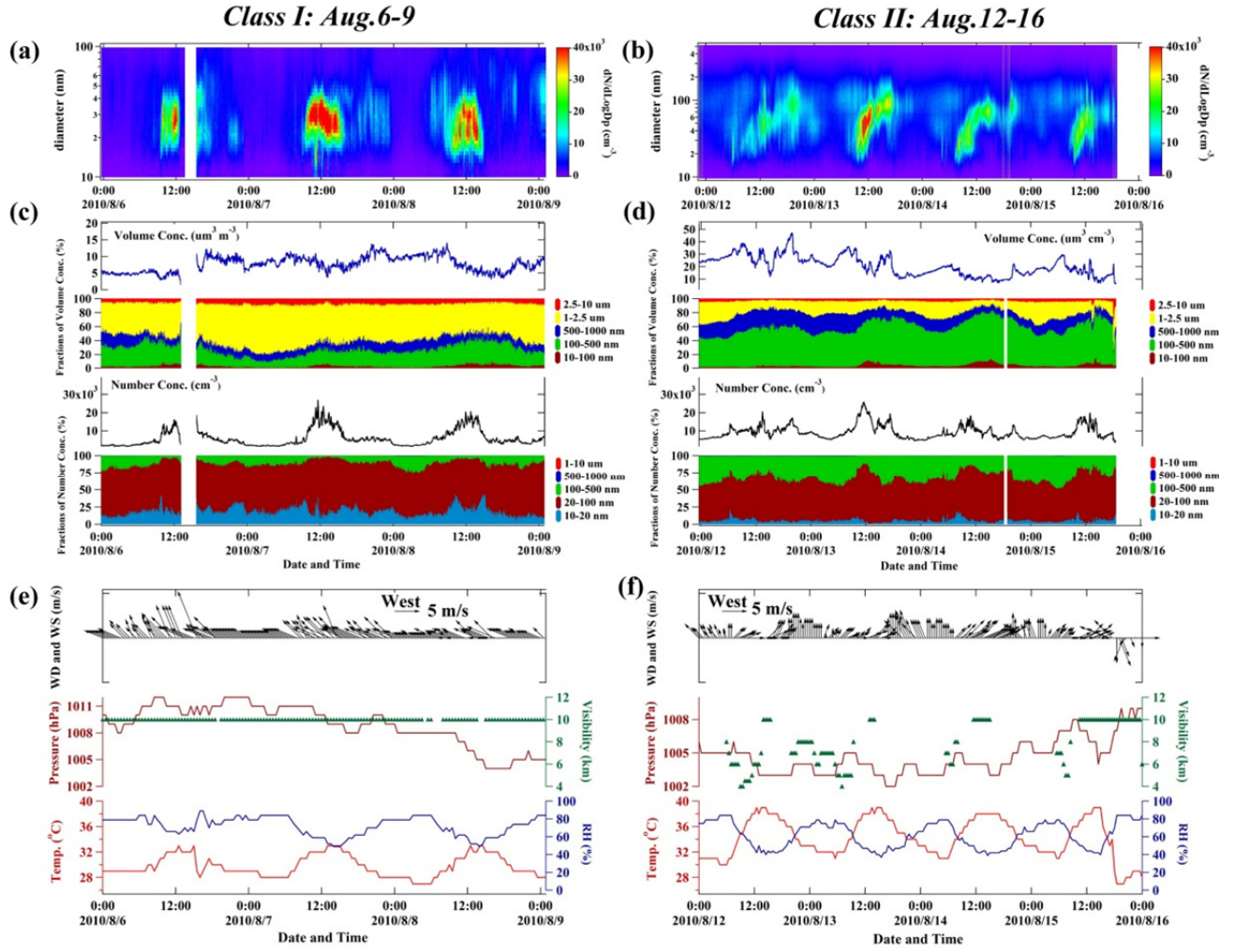

Fig. 6. Daily variations in (a, b) number size distributions; (c, d) number concentrations, volume concentrations and fractions of different particle size bins; and (e, f) meteorological parameters for 6–9 August and 12–16 August episodes.

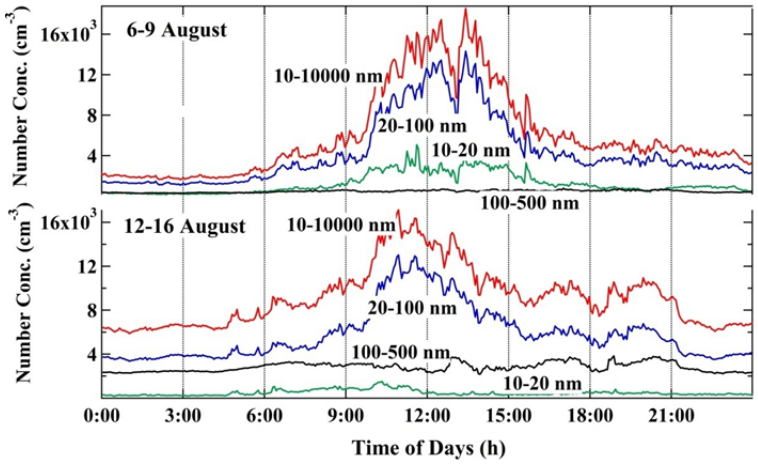

Fig. 7. Mean diurnal variations in particle number concentrations in size ranges 10–20 nm, 20–100 nm, 100–500 nm and 10–10000 nm.

midday was probably due to the particle formation and growth processes promoted by a strong photochemical process or specific anthropogenic sources.

During the 12–16 August episode (Class II), the particle growth processes exhibited a "banana shape" (Fig. 6(b)), indicating a significant time delay in the appearance of the

peak values of particle number concentrations (Fig. 6(d)). As during the Beijing Olympics 2008 (Gao *et al.*, 2012), few nucleation mode particles (10–20 nm) were observed (Fig. 6(d)). The Aitken and small-accumulation mode particles were the main contributors to the total particle number concentrations in this Class II episode, which had wider peaks (9:00–21:00) (Fig. 7). Compared to the 6–9 August (Class I) episode, this Class II episode (12–16 August) was characterized by lower visibility (4–10 km), lower pressure and higher temperatures (Figs. 6(e)–6(f)), which was probably beneficial to secondary aerosol formation and growth processes.

Trace gases such as SO_2, NO_2 and O_3 are useful indicators of the air quality in a region or city. SO_2 and NO_2 are the main precursors of sulfate and nitrate aerosols and O_3 plays an important role in atmospheric chemistry. The time series of NO_2, SO_2 and O_3 are shown in Figs. 8(a) and 8(b). On average, the concentrations of these trace gases in Class II episodes were 2–5 times higher than in Class I episodes. One obvious difference between Class I and Class II air quality was the extremely high O_3 concentrations in Class II, with peak values occurring at noon. The high O_3 concentrations were a result of photochemical reactions because O_3 is a secondary oxidation gaseous species in the troposphere, which helps to determine the oxidative capacity of the atmosphere.

NH_4^+, SO_4^{2-} and NO_3^- probably originated from secondary pollution particles produced by the transformation of their precursors, SO_2, NO_2 and NH_3 (Wang *et al.*, 2006). NH_4^+, SO_4^{2-}, NO_3^- and Cl^- were the dominant ions in Class I and Class II episodes, and together accounted for approximately 78% and 96% of the total water-soluble ions, respectively. To compare the major chemical compositions of the aerosols between air quality Classes I and II, we assumed that all of the existent sulfates in the particles were in the form of $(NH_4)_2SO_4$ (Matsumoto and Tanaka, 1996) and the excess part of ammonium was defined as ns-NH_4^+ (non-sulfate ammonium). The molar concentrations of ns-NH_4^+ were described using the following equation:

$$[\text{ns-NH}_4^+] = [\text{NH}_4^+] - 2 \times [\text{SO}_4^{2-}] \quad (1)$$

where [ns-NH_4^+], in units of μmol/m^3, is non-sulfate ammonium. [NH_4^+] and [SO_4^{2-}], in units of μmol/m^3, are the molar concentrations in $PM_{2.5}$.

Linear regression correlations between [NH_4^+] and [SO_4^{2-}] in the 6–9 August episode (Class I), and between [ns-NH_4^+] and [NO_3^-] in the 12–16 August episode (Class II) are shown in Figs. 8(e) and 8(f). The strong correlation between [NH_4^+] and [SO_4^{2-}] during the Class I episode (R^2 = 0.93) suggested that NH_4^+ was mainly present as $(NH_4)_2SO_4$. The slope and intercept of the regression function between [NH_4^+] and [SO_4^{2-}] were 0.95 and 0.02, revealing that NH_4^+ was not sufficient to couple SO_4^{2-} particles. In the Class II episode, [ns-NH_4^+] presented an extremely strong linear correlation with [NO_3^-] (R^2 = 0.96), indicating that NH_4^+ was mainly in the form of $(NH_4)_2SO_4$ and NH_4NO_3. The slope and intercept of the regression between [ns-NH_4^+] and [NO_3^-] were 0.72 and 0.05, suggesting an incomplete chemical coupling of NO_3^- by ns-NH_4^+ due to ammonia-poor aerosols. Our observations agreed with previous studies on aerosol ionic-chemistry (Wang *et al.*, 2006; Pathak *et al.*, 2009; Wang *et al.*, 2009; Du *et al.*, 2010). Pathak *et al.* (2009) found ammonia-poor aerosols in Shanghai and Beijing and Wang *et al.* (2009) confirmed that nitrate formation plays an important role in ammonia-poor aerosols. Du *et al.* (2010) noted that ammonia-poor aerosols exist in urban haze episodes. This study found that ammonia-poor aerosols exist not only in polluted air, but also in relatively clean air.

The sulfur oxidation ratio (SOR = n-SO_4^{2-}/(n-SO_4^{2-} + n-SO_2)) and nitrogen oxidation ratio (NOR = n-NO_3^-/(n-NO_3^- + n-NO_2)) are other available indicators that quantitatively characterize the secondary transformation reactions of SO_2 and NO_2, respectively. The variations in calculated SOR and NOR during the two episodes are shown in Fig. 9. The values of SOR for Class I and Class II episodes were all above 0.10. These values were comparable to previous studies showing that sulfate was mainly produced through the secondary transformation of SO_2 oxidation when SOR was above 0.10, whereas SOR was smaller than 0.10 under conditions of primary source emissions (Yao *et al.*, 2002; Fu *et al.*, 2008). As Fig. 9 shows, the SOR could reach up to 0.70 during the 12–16 August episode due to the secondary pollution and was relatively higher than that in Class I, indicating that secondary transformation was significant during both Class I and Class II episodes. Moreover, much higher SO_2 and NO_2 concentrations provided large amounts of precursors (Fig. 8(b)), which directly resulted in large amounts of secondary sulfate and nitrate in the atmosphere during Class II episodes.

CONCLUSION

This study characterized urban aerosols under the controlled local emission conditions that existed during the World Expo 2010 in Shanghai. The data were one month's worth of observations of aerosol number size distributions (10 nm–10 μm) and chemical compositions (1 h resolution) during August 2010. Back-trajectories and Lagrangian model analyses were combined to differentiate and compare the regional transport and local contributions.

Two classes of air quality were identified and compared through the analysis of particle number size distributions and chemical compositions. Class I represented the clear air conditions associated with ocean-oriented air masses. Particle counts in this type of air mass were dominated by particles in the size range 20–40 nm, and NH_4^+ was mainly present in the form of $(NH_4)_2SO_4$. As there were few nucleation mode particles (10 nm), the strong peak at noontime indicated that the particle formation or growth processes were promoted by the photochemical process or by specific anthropogenic sources. Class II air masses were dominated by regional transport pollution and by air masses originating in surrounding areas. Compared with Class I episodes, there was an increase of about 17 and 350% in particle number concentrations and total water soluble ions, respectively, in Class II episodes. The fraction of particles in the size range 50–200 nm increased sharply to almost 50% of the total particle count. An examination

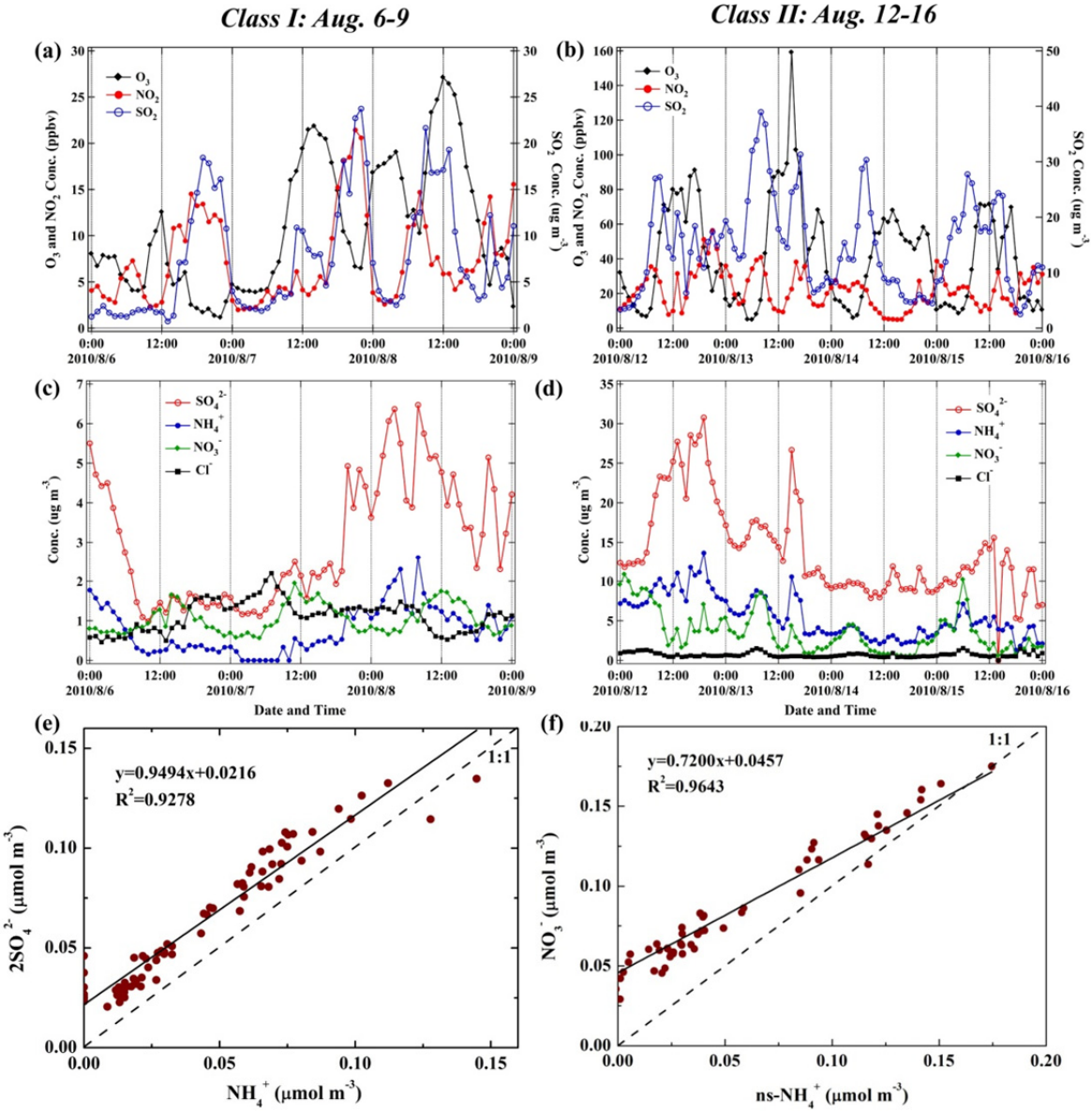

Fig. 8. Time series of traces gases (O_3, NO_2, SO_2) (a, b), water soluble ions (NH_4^+, SO_4^{2-}, NO_3^-, Cl^-) (c, d) and linear regression correlations between [NH_4^+] and [SO_4^{2-}] in the 6–9 August episode (Class I, left) and between [ns-NH_4^+] and [NO_3^-] in the 12–16 August episode (Class II, right).

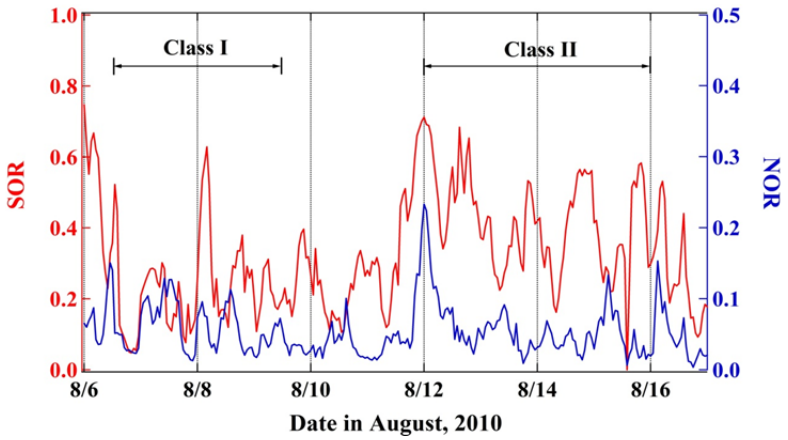

Fig. 9. Variations in the sulfur oxidation ratio (SOR) and nitrogen oxidation ratio (NOR) in August, 2010.

of the diurnal pattern and major water soluble ions suggested that the increase in size mode (50–200 nm) particles was probably due to the particle growth process. NH_4^+ was mainly in the form of $(NH_4)_2SO_4$ and NH_4NO_3.

Our results indicate that during the observation period, regional transport was responsible for the higher trace gases and particle volume concentrations, along with the large number of Aitken mode particles. These findings will help researchers and policy-makers understand the urban aerosol characteristics and the regional/local contributions to atmospheric fine particle pollution under the local emission control conditions that occurred during the Shanghai World Expo.

ACKNOWLEDGMENTS

This work was supported by the National Natural Science Foundation of China (Nos. 21190053, 21077025, 40875073, 41206027), the Science and Technology Commission of Shanghai Municipality (Nos. 10231203801, 10JC1401600), the open fund from the Key Laboratory of Data Analysis and Application, the State Oceanic Administration (No. GY02-2011-30-2), a General Financial Grant from the China Postdoctoral Science Foundation (2012M511460) and partly from the FP7 Project (No. n°069720).

REFERENCES

Chan, C.K. and Yao, X.H. (2008). Air Pollution in Mega Cities in China. *Atmos. Environ.* 42: 1–42.

Chow, J.C. and Watson, J.G. (1998). Guideline on Speciated Particulate Monitoring, Vol. 3–7, US EPA, p. 4–37.

De Foy, B., Varela, J.R., Molina, L.T. and Molina, M.J. (2006). Rapid ventilation of the Mexico City Basin and Regional Fate of the Urban Plume. *Atmos. Chem. Phys.* 6: 2321–2335.

Du, H.H., Kong, L.D., Cheng, T.T., Chen, J.M., Yang, X., Zhang, R.Y., Han, Z.W., Yan, Z. and Ma, Y.L. (2010). Insights into Ammonium Particle-to-gas Conversion: Non-sulfate Ammonium Coupling with Nitrate and Chloride. *Aerosol Air Qual. Res.* 10: 589–595.

Du, H.H., Kong, L.D., Cheng, T.T., Chen, J.M., Du, J.F., Li, L., Xia, X.G., Leng, C.P. and Huang, G.H. (2011). Insights into Summertime Haze Pollution Events over Shanghai Based on Online Water-Soluble Ionic Composition of Aerosols. *Atmos. Environ.* 45: 5131–5137.

Du, J.F., Cheng, T.T., Zhang, M., Chen, J.M., He, Q.S., Wang, X.M., Zhang, R.J., Tao, J., Huang, G.H., Li, X. and Zha, S.P. (2012). Aerosol Size Spectra and Particle Formation Events at Urban Shanghai in Eastern China. *Aerosol Air Qual. Res.* 12: 1362–1372.

Draxler, R.R. and Hess, G.D. (1998). An Overview of the HYSPLIT 4 Modeling System for Trajectories, Dispersion, and Deposition. *Aust. Meteorol. Mag.* 47: 295–308.

Feng, Y., Chen, Y., Guo, H., Zhi, G., Xiong, S., Li, J., Sheng, G. and Fu, J. (2009). Characteristics of Organic and Elemental Carbon in $PM_{2.5}$ Samples in Shanghai, China. *Atmos. Res.* 92: 434–442.

Fiebig, M., Lunder, C.R. and Stohl, A. (2009). Tracing Biomass Burning Aerosol from South America to Troll Research Station, Antarctica. *Geophys. Res. Lett.* 36: L14815, doi: 10.1029/2009GL038531.

Fu, H.B., Zhang, M., Li, W.J., Chen, J.M., Wang, L., Quan, X. and Wang, W.X. (2012). Morphology, Composition and Mixing State of Individual Carbonaceous Aerosol in Urban Shanghai. *Atmos. Chem. Phys.* 12: 693–707.

Fu, Q.Y., Zhuang, G.S., Wang, J., Xu, C., Huang, K., Li, J., Hou, B., Lu, T. and Streets, D.G. (2008). Mechanism of Formation of the Heaviest Pollution Episode ever Recorded in the Yangtze River Delta, China. *Atmos. Environ.* 42: 2023–2036.

Gao, J., Wang, T., Zhou, X.H., Wu, W.S. and Wang, W.X. (2009). Measurement of Aerosol Number Size Distributions in the Yangtze River Delta in China: Formation and Growth of Particles under Polluted Conditions. *Atmos. Environ.* 43: 829–836.

Gao, J., Chai, F.H., Wang, T. and Wang, W.X. (2011). Particle Number Size Distribution and New Particle Formation (NPF) in Lanzhou, Western China. *Particuology* 9: 611–618.

Gao, J., Chai, F.H., Wang, T., Wang, S.L. and Wang, W.X. (2012). Particle Number Size Distribution and New Particle Formation: New Characteristics during the Special Pollution Control Period in Beijing. *J. Environ. Sci.* 24: 14–21.

Gómez-Moreno, F.J., Pujadas, M., Plaza, J., Rodríguez-Maroto, J.J., Martínez-Lozano, P. and Artíñano, B. (2011). Influence of Seasonal Factors on the Atmospheric Particle Number Concentration and Size Distribution in Madrid. *Atmos. Environ.* 45: 3169–3180.

Hao, N., Valks, P., Loyola, D., Cheng, Y.F. and Zimmer, W. (2011). Space-based Measurements of Air Quality during the World Expo 2010 in Shanghai. *Environ. Res. Lett.* 6: 044004, doi: 10.1088/1748-9326/6/4/044004.

Huang, X.F., He, L.Y., Xue, L., Sun, T.L., Zeng, L.W., Gong, Z.H., Hu, M. and Zhu, T. (2012). Highly Time-resolved Chemical Characterization of Atmospheric Fine Particles during 2010 Shanghai World Expo. *Atmos. Chem. Phys. Discuss.* 12: 1093–1115.

Jia, X., Cheng, T.T., Chen, J.M., Xu, J.W and Chen, Y.H (2012). Columnar Optical Depth and Vertical Distribution of Aerosols over Shanghai. *Aerosol Air Qual. Res.* 12: 320–330.

Jongejan, P.A.C., Bai, Y., Veltkamp, A.C., Wyers, G.P. and Slanina, J. (1997). An Automated Field Instrument for the Determination of Acidic Gases in Air. *Int. J. Environ. Anal. Chem.* 66: 241–251.

Kan, H.D., London, S.J., Chen, G.H., Zhang, Y.H., Song, G.X., Zhao, N.Q., Jiang, L.L. and Chen, B.H. (2007). Differentiating the Effects of Fine and Coarse Particles on Daily Mortality in Shanghai, China. *Environ. Int.* 33: 376–384.

Khlystov, A., Wyers, G.P. and Slanina, J. (1995). The Steam-jet Aerosol Collector. *Atmos. Environ.* 29: 2229–2234.

Kulmala, M., Vehkamäki, H., Petäjä, T., Dal Maso, M., Lauri, A., Kerminen, V.M., Birmili, W. and McMurry, P.H. (2004). Formation and Growth Rates of Ultrafine Atmospheric Particles: A Review of Observations. *J.*

Aerosol Sci. 35: 143–176.

Li, H.Y., Han, Z.W., Cheng, T.T., Du, H.H., Kong, L.D., Chen, J.M., Zhang, R.J. and Wang, W.J. (2010). Agricultural Fire Impacts on the Air Quality of Shanghai during Summer Harvesttime. *Aerosol Air Qual. Res.* 10: 95–101.

Li, L., Chen, J.M., Chen, H., Yang, X., Tang, Y. and Zhang, R.Y. (2011). Monitoring Optical Properties of Aerosols with Cavity Ring-down Spectroscopy. *J. Aerosol Sci.* 42: 277–284.

Li, X.R., Wang, L.L., Wang, Y.S., Wen, T.X., Yang, Y.J., Zhao, Y.N. and Wang, Y.F. (2012). Chemical Composition and Size Distribution of Airborne Particle Matters in Beijing during the 2008 Olympics. *Atmos. Environ.* 50: 278–285.

Liu, B.Y.H., Romay, F.J., Dick, W.D., Woo, K.S. and Chiruta, M. (2010). A Wide-range Particle Spectrometer for Aerosol Measurement from 0.010 μm to 10 μm. *Aerosol Air Qual. Res.* 10: 125–139.

Matsumoto, K. and Tanaka, H. (1996). Formation and Dissociation of Atmospheric Particulate Nitrate and Chloride: An Approach Based on Phase Equilibrium. *Atmos. Environ.* 30: 639–648.

Mönkkönen, P., Koponen, I.K., Lehtinen, K.E.J., Hämeri, K., Uma, R. and Kulmala, M. (2005). Measurements in a Highly Polluted Asian Mega City: Observations of Aerosol Number Size Distribution, Modal Parameters and Nucleation Events. *Atmos. Chem. Phys.* 5: 57–66.

Ny, M.T. and Lee, B.K. (2011). Size Distribution of Airborne Particulate Matter and Associated Metallic Elements in an Urban Area of an Industrial City in Korea. *Aerosol Air Qual. Res.* 11: 643–653.

Okuda, T., Matsuura, S., Yamaguchi, D., Umemura, T., Hanada, E., Orihara, H., Tanaka, S., He, K.B., Ma, Y.L., Cheng, Y. and Liang, L.L. (2011). The impact of the Pollution Control Measures for the 2008 Beijing Olympic Games on the Chemical Composition of Aerosols. *Atmos. Environ.* 45: 2789–2794.

Palau, J.L., Pérez-Landa, G., Meliá, J., Segarra, D. and Millán, M.M. (2006). A Study of Dispersion in Complex Terrain under Winter Conditions Using High-resolution Mesoscale and Lagrangian Particle Models. *Atmos. Chem. Phys.* 6: 1105–1134.

Pathak, R.K., Wu, W.S. and Wang, T. (2009). Summertime $PM_{2.5}$ Ionic Species in Four Major Cities of China: Nitrate Formation in an Ammonia-deficient Atmosphere. *Atmos. Chem. Phys.* 9: 1711–1722.

Qu, W.J., Arimoto, R., Zhang, X.Y., Zhao, C.H., Wang, Y.Q. and Sheng, L.F. (2010). Spatial Distribution and Interannual Variation of Surface PM_{10} Concentrations over Eighty-six Chinese Cities. *Atmos. Chem. Phys.* 10: 5641–5662.

Quinn, P.K., Bates, T.S., Coffman, D., Onasch, T.B., Worsnop, D., Baynard, T., de Gouw, J.A., Goldan, P.D., Kuster, W.C., Williams, E., Roberts, J.M., Lerner, B., Stohl, A., Pettersson, A. and Lovejoy, E.R. (2006). Impacts of Sources and Aging on Submicrometer Aerosol Properties in the Marine Boundary Layer across the Gulf of Maine. *J. Geophys. Res.* 111: D23S36, doi: 10.1029/2006JD007582.

Seibert, P. and Frank, A. (2004). Source-receptor Matrix Calculation with a Lagrangian Particle Dispersion Model in Backward Mode. *Atmos. Chem. Phys.* 4: 51–63.

Stohl, A., Hittenberger, M. and Wotawa, G. (1998). Validation of the Lagrangian Particle Dispersion Model Flexpart Against Large Scale Tracer Experiment Data. *Atmos. Environ.* 32: 4245–4264.

Stohl, A., Foster, C., Eckhardt, S., Spichtinger, N., Huntrieser, H., Heland, J., Schlager, H., Wilhelm, S., Arnold, F. and Cooper, O. (2003). A Backward Modeling Study of Intercontinental Pollution Transport Using Aircraft Measurements. *J. Geophys. Res.* 108: 4370, doi: 10.1029/2002JD002862.

Stohl, A., Foster, C., Frank, A., Seibert, P. and Wotawa, G. (2005). Technical Note: The Lagrangian Particle Dispersion Model FLEXPART Version 6.2. *Atmos. Chem. Phys.* 5: 2461–2474.

Streets, D.G., Yu, C., Wu, Y., Chin, M., Zhao, Z., Hayasaka, T. and Shi, G. (2008). Aerosol Trends over China, 1980-2000. *Atmos. Res.* 88: 174–182.

Tie, X., Brasseur, G., Zhao, C., Granier, C., Massie, S., Qin, Y., Wang, P.C., Wang, G.L. and Yang, P.C. (2006). Chemical Characterization of Air Pollution in Eastern China and the Eastern United States. *Atmos. Environ.* 40: 2607–2625.

Tsai, H.H, Yuan, C.S., Hung, C.H. and Lin, C. (2011). Physicochemical Properties of $PM_{2.5}$ and $PM_{2.5-10}$ at Inland and offshore Sites over Southeastern Coastal Region of Taiwan Strait. *Aerosol Air Qual. Res.* 11: 664–678.

UNEP (United Nations Environment Programme) (2010). UNEP Environmental Assessment: Expo 2010 Shanghai, China (Nairobi: UNEP)

Van der, A.R.J., Peters, D.H.M.U., Eskes, H., Boersma, K.F., Van Roozendael, M., De Smedt, I. and Kelder, H.M. (2006). Detection of the Trend and Seasonal Variation in Tropospheric NO_2 over China. *J. Geophys. Res.* 111, D12317, doi: 10.1029/2005JD006594.

Wang, X., Westerdahl, D., Chen, L.C., Wu, Y., Hao, J.M., Pan, X.C., Guo, X.B. and Zhang, K.M. (2009a). Evaluating the Air Quality Impacts of the 2008 Beijing Olympic Games: On-road Emission Factors and Black Carbon Profiles. *Atmos. Environ.* 43: 4535–4543.

Wang, W.T., Primbs, T., Tao, S. and Simonich, S.M. (2009b). Atmospheric Particle Matter Pollution during the 2008 Beijing Olymics. *Environ. Sci. Technol.* 43: 5314–5320.

Wang, X.F., Zhang, Y.P., Chen, H., Yang, X., Chen, J.M. and Geng, F.H. (2009). Particulate Nitrate Formation in a Highly Polluted Urban Area: A Case Study by Single-particle Mass Spectrometry in Shanghai. *Environ. Sci. Technol.* 43: 3061–3066.

Wang, X.F., Gao, S., Yang, X., Chen, H., Chen, J.M., Zhuang, G.S., Surratt, J.D., Chan, M.N. and Seinfeld, J.H. (2010). Evidence for High Molecular Weight Nitrogen-containing Organic Salts in Urban Aerosols. *Environ. Sci. Technol.* 44: 4441–4446.

Wang, Y., Zhuang, G.S., Zhang, X.Y., Huang, K., Xu, C., Tang, A.H., Chen, J.M. and An, Z.S. (2006). The Ion Chemistry, Seasonal Cycle, and Sources of $PM_{2.5}$ and TSP

Aerosol in Shanghai. *Atmos. Environ.* 40: 2935–2952.

Yang, F., Chen, H., Wang, X.N., Yang, X., Du, J.F. and Chen, J.M. (2009). Single Particle Mass Spectrometry of Oxalic Acid in Ambient Aerosols in Shanghai: Mixing State and Formation Mechanism. *Atmos. Environ.* 43: 3876–3882.

Yao, X.H., Chan, C.K., Fang, M., Cadle, S., Chan, T., Mulawa, P., He, K. and Ye, B. (2002). The Water-soluble Ionic Composition of $PM_{2.5}$ in Shanghai and Beijing, China. *Atmos. Environ.* 36: 4223–4234.

Ye, B.M., Ji, X.L., Yang, H.Z., Yao, X.H., Chan, C.K., Cadle, S.H., Chan, T. and Mulawa, P. A. (2003). Concentration and Chemical Composition of $PM_{2.5}$ in Shanghai for a 1-year Period. *Atmos. Environ.* 37: 499–510.

Ye, X.N., Ma, Z., Hu, D.W., Yang, X. and Chen, J.M. (2011). Size-resolved Hygroscopicity of Submicrometer Urban Aerosols in Shanghai during Wintertime. *Atmos. Res.* 99: 353–364.

Zhang, H.F., Ye, X.N., Cheng, T.T., Chen, J.M., Yang, X., Wang, L. and Zhang, R.Y. (2008). A Laboratory Study of Agricultural Crop Residue Combustion in China: Emission Factors and Emission Inventory. *Atmos. Environ.* 42: 8432–8441.

Zhang, H.F., Hu, D.W., Chen, J.M., Ye, X.N., Wang, S.X., Hao, J.M., Wang, L., Zhang, R.Y. and An, Z.S. (2011). Particle Size Distribution and Polycyclic Aromatic Hydrocarbons Emissions from Agricultural Crop Residue Burning. *Environ. Sci. Technol.* 45: 5477–5482.

Zhang, M., Wang, X.M., Chen, J.M., Cheng, T.T., Wang, T., Yang, X., Gong, Y.G., Geng, F.H. and Chen, C.H. (2010). Physical Characterization of Aerosol Particles during the Chinese New Year's Firework Events. *Atmos. Environ.* 44: 5191–5198.

Zhou, Y., Wu, Y., Yang, L., Fu, L.X., He, K.B., Wang, S.X., Hao, J.M., Chen, J.C. and Li, C.Y. (2010). The Impact of Transportation Control Measures on Emission Reductions during the 2008 Olympic Games in Beijing, China. *Atmos. Environ.* 44: 285–293.

Received for review, February 3, 2012
Accepted, September 3, 2012